ORIGINAL PAPER

Amyloid-β pathology enhances pathological fibrillary tau seeding induced by Alzheimer PHF in vivo

Cristina Vergara[1] · Sarah Houben[1] · Valérie Suain[1] · Zehra Yilmaz[1] · Robert De Decker[1] · Virginie Vanden Dries[1] · Alain Boom[1] · Salwa Mansour[1] · Karelle Leroy[1] · Kunie Ando[1] · Jean-Pierre Brion[1]

Abstract

Neuropathological analysis in Alzheimer's disease (AD) and experimental evidence in transgenic models overexpressing frontotemporal dementia with Parkinsonism linked to chromosome 17 (FTDP-17) mutant tau suggest that amyloid-β pathology enhances the development of tau pathology. In this work, we analyzed this interaction independently of the overexpression of an FTDP-17 mutant tau, by analyzing tau pathology in wild-type (WT), 5xFAD, APP$^{-/-}$ and tau$^{-/-}$ mice after stereotaxic injection in the somatosensory cortex of short-length native human AD-PHF. Gallyas and phosphotau-positive tau inclusions developed in WT, 5xFAD, and APP$^{-/-}$ but not in tau$^{-/-}$ mice. Ultrastructural analysis demonstrated their intracellular localization and that they were composed of straight filaments. These seeded tau inclusions were composed only of endogenous murine tau exhibiting a tau antigenic profile similar to tau aggregates in AD. Insoluble tau level was higher and ipsilateral anteroposterior and contralateral cortical spreading of tau inclusions was more important in AD-PHF-injected 5xFAD mice than in WT mice. The formation of large plaque-associated dystrophic neurites positive for oligomeric and phosphotau was observed in 5xFAD mice injected with AD-PHF but never in control-injected or in non-injected 5xFAD mice. An increased level of the p25 activator of CDK5 kinase was found in AD-PHF-injected 5xFAD mice. These data demonstrate in vivo that the presence of Aβ pathology enhances experimentally induced tau seeding of endogenous, wild-type tau expressed at physiological level, and demonstrate the fibrillar nature of heterotopically seeded endogenous tau. These observations further support the hypothesis that Aβ enhances tau pathology development in AD through increased pathological tau spreading.

Keywords Paired helical filaments · Neurofibrillary tangles · Aβ · Prion-like tau propagation · Tau seeding · Alzheimer's disease

Introduction

Alzheimer's disease (AD) is characterized by two defining neuropathological hallmarks: senile plaques consisting of aggregates of amyloid-β (Aβ) peptide surrounded by dystrophic neurites (DN) and neurofibrillary tangles (NFTs) formed by bundles of paired helical filaments (PHF)

✉ Jean-Pierre Brion
  jpbrion@ulb.ac.be

1   Laboratory of Histology, Neuroanatomy
    and Neuropathology, UNI (ULB Neuroscience Institute),
    Faculty of Medicine, Université Libre de Bruxelles, 808,
    route de Lennik, Bldg GE, 1070 Brussels, Belgium

composed of the microtubule-associated protein tau in an aggregated form [18]. The latter lesion is strongly correlated with the degree of cognitive impairment [42]. Although the brain distribution of these two lesions does not show neuroanatomical overlap at early stages of the disease, both neuropathological and experimental evidence suggest the existence of a cross talk modulating the development of both lesions. Injection of Aβ fibrils [23] or Aβ-containing brain extract [5] into mutant tau transgenic mice or crossing between mutant tau and APP or 5xFAD transgenic mice exacerbated tau pathology (e.g., [4, 5, 27, 28, 36, 47, 48, 50, 51, 55]).

The mechanisms leading to this enhanced tau pathology are not well understood. The expansion of tau pathology in the brain during progression of AD follows a relatively systematic scheme suggesting that tau pathology progresses by following neuroanatomically connected areas [7], possibly

through synaptically connected neurons. Strong experimental evidence indicates that tau aggregation can be seeded in cells (for review, see Ref. [40]) and transmitted from one cell to another, both in vitro and in vivo, in transgenic models overexpressing wild-type or mutant tau [10, 49]. We previously showed that human native PHF extracted from sporadic AD brain (AD-PHF) induced tau aggregation and propagation in the form of argyrophilic grains composed of hyperphosphorylated endogenous murine tau in wild-type (WT) mouse brains [3]. Such PHF contain the six human wild-type tau isoforms as well as all post-translational modifications characteristic of PHF from AD brains. AD-PHF recruits endogenously expressed non-mutant tau in WT mice [3, 24] representing a closer model to the human pathological condition than transgenic tau models overexpressing mutant tau. In the present study, we provide evidence that Aβ increases endogenous wild-type tau seeding through enhancement of tau propagation, as well as the ultrastructural demonstration that the in vivo induced tau aggregates are composed of bundles of tau filaments.

Materials and methods

Human brain tissue

Human brain tissue samples were taken at autopsy from three demented patients clinically diagnosed as AD cases and from two non-demented control subjects. Tissue samples were fixed with formalin 10% and embedded in paraffin for neuropathological examination or were kept at −80 °C. The neuropathological examination confirmed the presence of numerous NFTs and amyloid plaques in the AD cases (Braak stage VI, Thal stages 3–5) and their absence in the control cases (Supplementary Table 1). This study on postmortem brain tissue was performed in compliance and following approval of the Ethical Committee of the Medical School of the Free University of Brussels.

Mouse lines

The 5xFAD double transgenic mice co-express and co-inherit the 695 amino acids isoform of the human amyloid precursor protein (APP695) carrying the Swedish, Florida, and London mutations and the human presenilin-1 (PS1) carrying the M146L and L286 V mutations (Tg6799 line) [44]. The APP-deficient mouse line [59] and the tau$^{-/-}$ mouse line [56] were obtained from Jackson Laboratories (Bar Harbor, ME, USA). All mouse lines were maintained on C57Bl/6 J genetic background and only 5xFAD heterozygous transgenic mice were used for

this study. Genotyping was performed by PCR amplification of genomic DNA as reported previously [27, 35].

Preparation and characterization of Sarkosyl-insoluble PHF fraction

Sarkosyl fractionation of human brain tissue was carried out as previously described [3, 8]. 0.5 g of frozen frontal cortex from control and AD cases was homogenized in 10 volumes of ice-cold PHF-extraction buffer (10 mM Tris–HCl (pH 7.4), 0.8 M NaCl, 1 mM EDTA, 10% sucrose). The homogenate was centrifuged at 15,000×g for 20 min at 4 °C. N-lauroylsarcosine sodium salt (L-5125; Sigma-Aldrich) was added to the supernatant to reach a final concentration of 1% (w/v). The lysate was incubated at 4 °C overnight with a mild agitation followed by an ultracentrifugation at 180,000×g for 30 min at 4 °C. The Sarkosyl soluble supernatant was removed and the Sarkosyl-insoluble pellet containing PHF was gently rinsed and re-suspended in 0.25 ml of PBS by vigorous pipetting. The protein concentration was determined by Bradford protein assay (Bio-Rad) and adjusted to 1 µg/µl. This Sarkosyl-insoluble PHF-tau fraction was aliquoted and kept at −80 °C.

For ultrastructural characterization of AD-PHF by transmission electron microscopy, Sarkosyl-insoluble material was adsorbed on formvar-carbon-coated EM grids and negatively stained with potassium phosphotungstate as reported [8] before observation with a Zeiss EM 809T at 80 kV. The yield of PHF-tau proteins in the Sarkosyl-insoluble fraction was assessed by reference to a standard curve generated using recombinant tau proteins obtained from bacterial culture (see Electronic supplementary material for methods) and of known tau concentrations. Different dilutions of recombinant tau and of the freshly obtained AD-PHF were loaded in a 10% Tris–glycine gel, transferred on a nitrocellulose membrane and immunoblotted with the B19 anti-total tau antibody. The optical density (OD) of the resulting bands was measured using image J software and a standard curve was generated using the known concentrations of the recombinant tau. Tau immunodepletion of Sarkosyl-insoluble fractions was performed using the BR21 anti-human tau antibody (see Electronic supplementary material for methods). To assess protease resistance of PHF-tau from AD cases, Sarkosyl soluble and insoluble material was digested with proteinase K as described [19]. Briefly, samples were digested with 0–10 µg/ml proteinase K in PBS for 30 min at 21 °C. Digestion was stopped using 5 mM PMSF. Samples were heated in Laemmli buffer at 100 °C for 5 min and were analyzed by western blot using anti-tau B19 and anti-phosphotau PHF1 antibodies.

Stereotaxic brain injection

Six-month-old WT C57/BL6, 5xFAD, APP$^{-/-}$ and tau$^{-/-}$ mice were injected with Sarkosyl-insoluble fractions from AD cases (WT $n = 12$, 5xFAD $n = 18$, APP$^{-/-}$ $n = 3$, tau$^{-/-}$ $n = 2$), tau-immunodepleted AD cases (WT $n = 1$, 5xFAD $n = 1$) and control cases (WT $n = 24$, 5xFAD $n = 16$). Unilateral stereotaxic injections were performed using a stereotaxic apparatus (Kopf Instruments) [3] in the left primary somatosensory cortex (rostro-caudal -1.46 mm; lateral $+0.15$ mm; depth -0.10 mm). 1 µg of Sarkosyl-insoluble material was injected at the concentration of 1 µg/µl at a speed of 0.1 µl/min with a pump (kdScientific), using a 200 µm diameter needle (Thermofisher). The needle was gently removed 5 min after injection. Mice were killed 3 months after injection. All studies on animals were performed in compliance with and after approval of the Ethical committee for the care and use of laboratory animals of the Medical School of the Free University of Brussels.

Spatial memory testing

Wild-type and 5xFAD mice injected with control or AD-PHF fractions were tested in the Y-maze for spontaneous alternations 3 months after injection, as described previously [34] (see Electronic supplementary material for methods).

Brain homogenization

Mice brain was dissected and homogenized as reported [2] in 10 volumes of ice-cold modified RIPA buffer containing 50 mM Tris pH 7.4 supplemented with 150 mM NaCl, 1% NP40, 0.25% sodium deoxycholate, 5 mM EDTA, 1 mM EGTA, Roche complete protease inhibitors, 1 mM PMSF, and phosphatase inhibitor cocktail 2, (SIGMA P-5726) and incubated for 60 min at 4 °C on a rotator. The homogenate was centrifuged (20,000×g for 20 min at 4 °C) and the supernatant was used as an RIPA soluble fraction. The RIPA-insoluble pellet was re-suspended in fivefold volume of 8 M urea supplemented with 5 mM EDTA, 1 mM EGTA, Roche complete protease inhibitors, and phosphatase inhibitor cocktail 2 (P-5726, SIGMA) by vortexing and sonication on ice and incubated for 30 min at room temperature on a rotator. The mixture was centrifuged at 20,000×g at 4 °C for 20 min. The supernatant was used as an RIPA-insoluble fraction. Fractions were analyzed by SDS-PAGE and immunoblotting (see Electronic supplementary material for methods and antibodies).

Histological staining and immunolabeling

Mice were killed by cervical dislocation and brains were fixed in 10% (v/v) formalin for 24 h before embedding them in paraffin. Tissue sections (10 µm thick) were stained with the Gallyas silver-staining method to identify aggregated tau inclusions and with Congo Red to visualize amyloid deposits enriched in β-sheets structure. The immunohistochemical labeling was performed using the ABC method. Briefly, tissue sections were treated with H_2O_2 to inhibit endogenous peroxidase and incubated with the blocking solution (10% (v/v) normal horse serum in TBS). After an overnight incubation with the diluted primary antibody, the sections were sequentially incubated with either horse anti-mouse or goat anti-rabbit antibodies conjugated to biotin (Vector) followed by the ABC complex (Vector Laboratories). The peroxidase activity was developed using diaminobenzidine (DAB) as chromogen. Double immunolabeling was performed using fluorescent markers followed by nuclear DAPI staining. The first antibody was detected using an anti-rabbit IgG conjugated to HRP (#7074, Cell signaling) and revealed with Tyramide-FITC (Perkin Elmer). The second antibody was detected using an anti-mouse antibody conjugated to biotin, followed by streptavidin conjugated to Alexa 594 (Molecular Probes). Slides were examined with an Axioplan microscope (Zeiss) and an Axiovert 200 M microscope (Zeiss) and digital images were acquired using an Axiocam HRc camera. The 3D-association between amyloid and tau pathologies was analyzed using the CUBIC method for tissue clarification [52] with a slight modification [1] as detailed in electronic supplementary material.

Ultrastructural analysis and immunolabeling in electron microscopy

As reported [27], anesthetized mice were transcardially perfused with a solution of 2% (w/v) paraformaldehyde and 2% (v/v) glutaraldehyde in 0.1 M phosphate buffer at pH 7.4. After dissection and further fixation in 4% (w/v) glutaraldehyde in 0.1 M phosphate buffer at pH 7.4 for 90 min, the tissue blocks were post-fixed in 2% (w/v) OsO_4 for 30 min, dehydrated and embedded in Epon. Ultrathin sections of the cerebral cortex were counterstained with uranyl acetate and lead citrate for further observation with a Zeiss EM 809T at 80 kV. For immunolabeling in electron microscopy, mice were transcardially perfused with a solution of 4% (w/v) paraformaldehyde and 0.5% (v/v) glutaraldehyde in 0.1 M phosphate buffer at pH 7.4. Tissue blocks of the cerebral cortex were cut in 50 µm thick sections using a Vibratome and immunolabeling performed with the ABC method as reported [39], using the rabbit B19 anti-tau antibody as primary antibody, an anti-rabbit antibody conjugated to biotin (Vector) and the ABC complex (Vector). The peroxidase activity was revealed using DAB as chromogen. The labeled tissue sections were post-fixed in 2% (w/v) OsO_4 and processed as described above.

Analysis of tau spreading and association with amyloid deposits

To quantify the extent of tau pathology, the size and area covered by tau-positive structures after immunolabeling with the B19 anti-tau antibody were first measured for each mouse in a rectangular area covering the whole thickness of the cortex at the level of the injection site, by thresholding analysis on digital images using the NIH ImageJ software, as reported [57]. The anteroposterior distribution of tau pathology was next analyzed on serial coronal sections immunolabeled with the B19 anti-tau antibody. The length between the maximal anterior and posterior coronal levels where a tau pathology could be detected was defined as the anteroposterior propagation. The mathematical mean of these lengths in each mouse cohort was defined as the mean anteroposterior propagation of tau pathology in these mice. A semi-quantitative evaluation of the distribution and density of tau pathology was also performed on these coronal sections to generate heat maps with a color coding system. The relationship of tau-positive structures with Aβ deposits was assessed after double immunolabeling with the anti-tau B19 and anti-Aβ 6E10 antibodies, by measuring, in the rectangular area covering the whole thickness of the cortex at the level of the injection site, the area covered by tau-positive processes in a surface centered on an Aβ deposit (for at least 25 amyloid plaques in each mouse) and extending from 20 μm at the border of the Aβ deposit. The area covered by Aβ deposits was also measured in the whole thickness of the cortex in the same rectangular area by thresholding analysis using the NIH ImageJ software.

Statistical analysis

Statistical analysis was performed using the Prism program (Graphpad Software). Statistical comparisons were performed using unpaired two-tailed Student t tests, Fisher's tests for contingency analysis and two-way ANOVA as noted in figure legends. Values of $P < 0.05$ were considered significant.

Results

Characterization of human AD-PHF fractions

Western blotting analysis after denaturing SDS-PAGE of Sarkosyl-insoluble PHF fractions from AD cases showed the characteristic three main PHF tau species (Fig. 1a); these fractions were devoid of Aβ immunoreactivity [3]. Negative staining in electron microscopy of PHF fractions revealed numerous PHF (Fig. 1b) with an average length of $180.9 \text{ nm} \pm 8.4 \text{ nm}$ (mean ± SEM). The frequency

distribution of PHF lengths was relatively similar in the three AD cases used in this study (Suppl. Figure 1). AD-PHF from case 2 had the highest yield of Sarkosyl-insoluble PHF and was principally used throughout this study. Tau was not detected in the Sarkosyl-insoluble fraction from the control brains (Fig. 1a) and after immunodepletion of tau from Sarkosyl-insoluble fraction from AD patients with the BR21 anti-human tau antibody (Suppl. Figure 3c). After proteinase K digestion, tau proteins were strongly decreased in the Sarkosyl-soluble supernatant from control and AD cases. In contrast, PHF-tau in the Sarkosyl-insoluble fractions from AD cases showed partial resistance to proteinase K digestion up to 5 μg/ml (Fig. 1c). Proteinase K digestion of AD-PHF generated two major lower tau fragments between 15 and 20 kDa. The estimated yield of PHF protein in PHF fractions (in protein weight) was of 40–65% after solubilization in sample buffer for SDS-PAGE and using recombinant tau for generating a standard curve.

AD-PHF-injected 5xFAD mice exhibit a working memory deficit compared to WT mice

Control fraction or AD-PHF was injected in the cortex of WT and 5xFAD mice at 6 months. Numerous amyloid plaques are present in the cortex of 5xFAD at this age. 3 months after injection, spatial working memory was tested by Y-maze test for spontaneous alternations in WT and 5xFAD mice injected with AD-PHF or control fraction. A significant overall effect of the genotype was observed by two-way ANOVA ($P = 0.0056$). AD-PHF-injected 5xFAD mice had a significant decreased ratio of spontaneous alternations compared to AD-PHF injected WT mice ($P < 0.05$), by Bonferroni post-tests (Suppl. Figure 2).

AD-PHF induces aggregation of murine tau into Gallyas and tau-positive grains and neuropil threads into both WT and 5xFAD mice
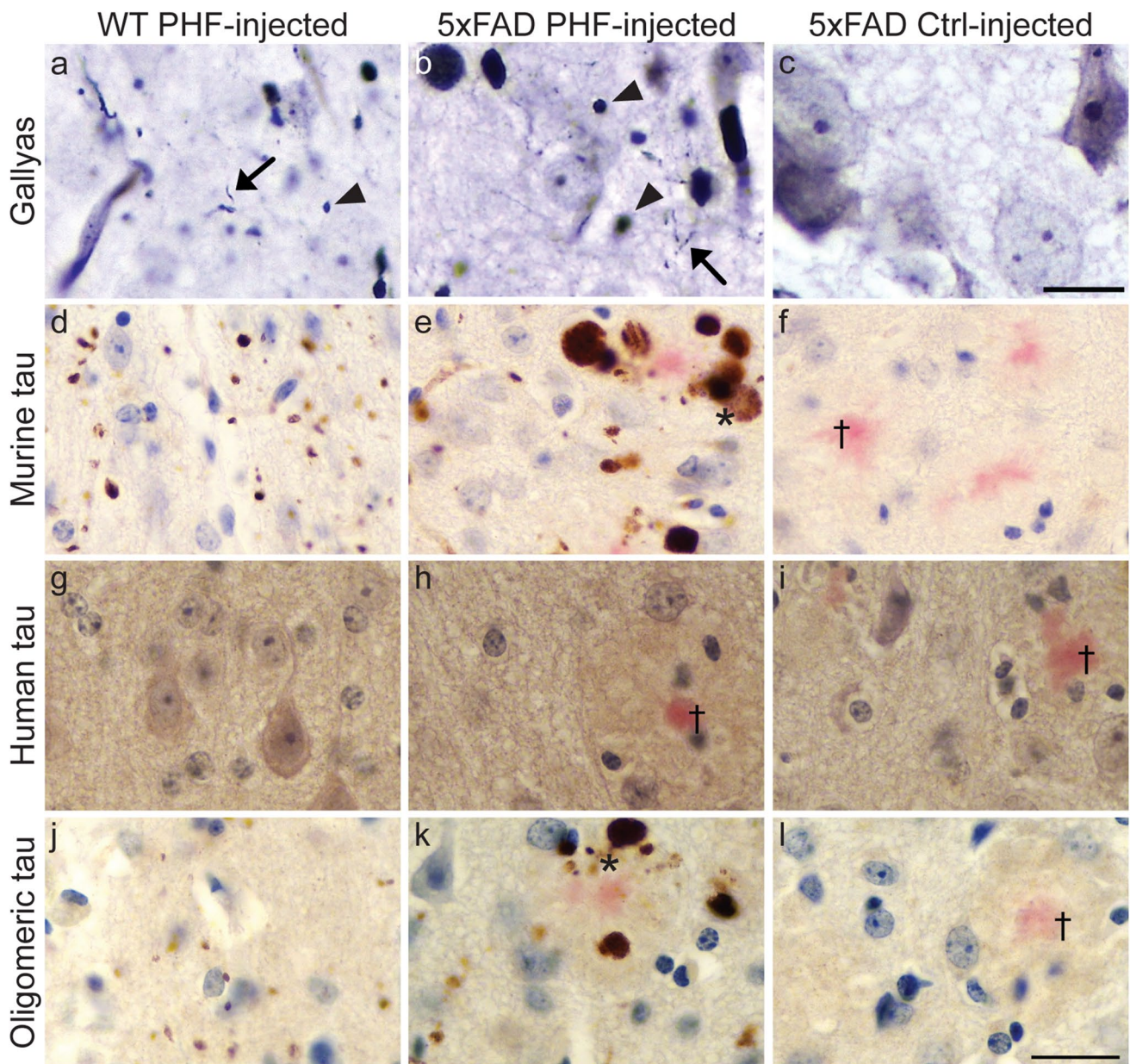
Stereotaxic injection of human AD-PHF induced the appearance of Gallyas-positive grains and neuropil threads (NT) in the cortex of WT and 5xFAD mice 3 months after injection (Fig. 2a, b), which were positive with the murine tau antibody (Fig. 2d, e) but not with the human tau BR21 antibody (Fig. 2g, h). After this 3-month incubation period, the injected human material was no longer detected, as previously reported [3]. These tau inclusions were labeled with a panel of antibodies specific for phosphotau (AT8, pSer422, PHF1), conformationally altered tau (AT100, Alz50, MC1), recapitulating the antigenic profile of NFT in AD (Table 1; Fig. 3). They were labeled with the anti-4R tau, but not with anti-3R tau antibodies, as only 4R tau isoforms are expressed in adult mouse neurons. Tau inclusions were not labeled with the anti-Aβ
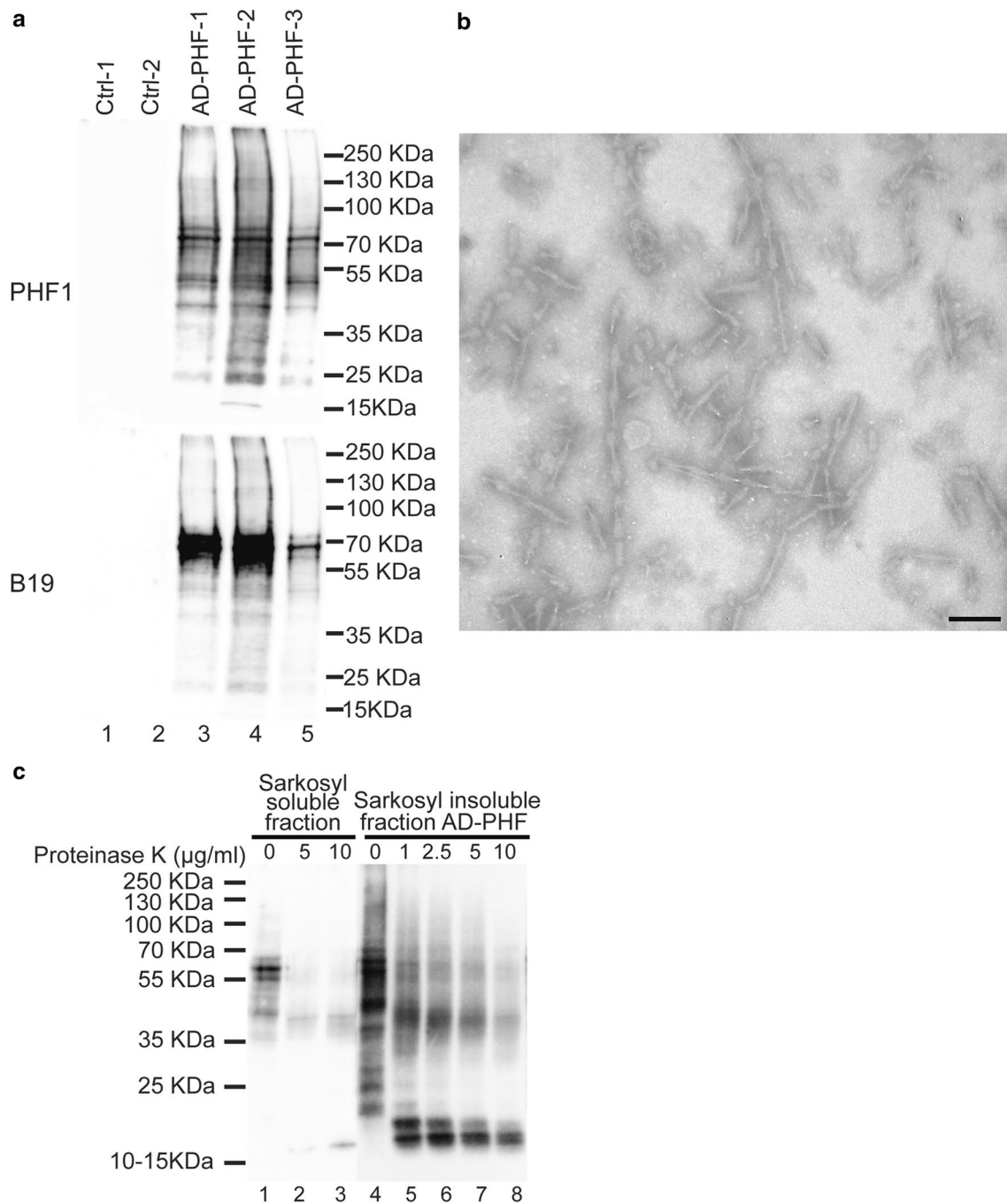
Fig. 1 Characterization of Sarkosyl insoluble human PHF from AD patients. **a** Western blot analysis of Sarkosyl-insoluble human PHF using anti-phosphotau antibody PHF1 and pan tau antibody B19. After SDS-PAGE in denaturing conditions, PHF-tau proteins from the three AD cases (lanes 3, 4, 5) used in this study had a similar migration pattern, with three main species of 64–72 kDa. The Sarkosyl fractions prepared from the two control subjects (lanes 1 and 2) did not contain any tau immunoreactivity. **b** Transmission electron microscopy (TEM) analysis of AD-PHF by negative staining shows that the Sarkosyl fraction from AD cases contained numerous short-length PHFs. Scale bar 50 nm. **c** Western blot analysis (B19 tau anti-body) after proteinase K digestion of soluble and Sarkosyl-insoluble fractions from AD patients (after SDS-PAGE). Lanes 1, 2, 3: soluble fraction from AD case 110 was digested with proteinase K at 0, 5 or 10 µg/ml. Soluble tau contained three main PHF-tau species of 64–72 kDa but these tau species were completely digested with proteinase K at 5 µg/ml. Lanes 4–8: Sarkosyl insoluble fraction from AD was digested with proteinase K at 0, 1, 2.5, 5 or 10 µg/ml. The 64–72 kDa insoluble PHF-tau species showed partial resistance to proteolytic digestion. Proteinase K digestion generated two major lower tau fragments between 15 and 20 kDa

Fig. 2 Injection of human AD-PHF induces seeding and aggregation of murine tau. **a–c** Gallyas-positive grains (arrowheads) and neuropil threads (arrows) were observed in the cortex of WT ($n=6$) (**a**) and 5xFAD ($n=7$) (**b**) mice, both injected with AD-PHF, but not in control-injected 5xFAD mice ($n=3$) (**c**). **d–f** Those granular structures were labeled with the murine tau-specific mTau5 antibody in AD-PHF-injected WT (**d**) and 5xFAD (**e**) mice. This antibody labeled plaque-associated DN in AD-PHF-injected 5xFAD mice (**e**) but not in control-injected 5xFAD mice (**f**). **g–l** Grains in WT (**g**, **j**) and 5xFAD (**h**, **k**) mice, both injected with AD-PHF, and plaque-associated DN in AD-PHF-injected 5xFAD mice (**h**, **k**) were not labeled with the human tau specific antibody BR21 (**g–i**) but were labeled with the T22 anti-oligomeric tau antibody (**j–l**). **d–l** Hematoxylin and Congo Red counterstaining. Asterisks indicate plaque-associated DN. Crosses indicate Congo red-positive dense core of amyloid plaques. Scale bar: **a–c** 10 μm; **d–l** 20 μm

antibodies. These results were similar in mice injected with PHF independently prepared from the three AD cases. Injection of AD-PHF in APP$^{-/-}$ mice also induced tau-positive inclusions (Suppl. Figure 3a), suggesting that the presence of murine APP or its derivatives is not necessary for tau aggregation in these mice. Injection of Sarkosyl-insoluble material from the control brain did not induce any detectable tau pathology at 9 months (Fig. 2f, l). In addition, injection of tau-immunodepleted AD-PHF did not generate these tau inclusions (Suppl. Figure 3d, e). In tau$^{-/-}$ mice, injection of AD-PHF did not induce a tau pathology (Suppl. Figure 3b). These data thus indicate that human PHF induced aggregation of endogenous 4R murine tau in both WT and 5xFAD mice, also conferring

Table 1 Immunoreactivity of tau inclusions and plaque-associated dystrophic neurites

Antibody	Epitope	WT AD-PHF grains	5xFAD AD-PHF grains	5xFAD AD-PHF DN
B19	Total tau	+	+	+
mTau5	Murine tau	+	+	+
BR21	Human tau	–	–	–
RD3	3R tau	–	–	–
RD4	4R tau	+	+	+
AT100	pT212/T214	+	+	+
AT8	pS202/T205	+	+	+
PHF1	pS396/S404	+	+	+
MC1	7–9 and 312–342	+	+	+
Alz50	2–10 and 312–342	+	+	+
pSer422	pS422	+	+	+
T22	Oligo tau	+	+	+
Gallyas staining	β-Sheet	+	+	–
Aβ42		–	–	–
Ubiquitin		+	+	+
p62	C-term of p62	+	+	(+)

Tau inclusions and DN were positive for pan tau B19 and murine tau antibodies as well as 4R tau, but not for human tau or 3R tau, in both WT ($n = 6$) and 5xFAD ($n = 7$) mice, injected with AD-PHF. The inclusions and DN were positively labeled with a panel of phosphotau antibodies and conformation dependent tau antibodies. On the contrary, DN were not positive for Gallyas staining but they were positive for T22 labeling oligomeric tau. Both inclusions and DN were also positive for ubiquitin and p62, although p62 staining in DN was weaker

DN plaque-associated dystrophic neurites

them a phosphotau and abnormal conformational antigenic profile similar to tau aggregates in AD and 4R tauopathies.

AD-PHF induces accumulation of oligomeric murine tau into plaque-associated dystrophic neurites

Aβ-positive cores in amyloid plaques in 5xFAD mice are surrounded by a corona of large dystrophic neurites strongly labeled by anti-APP antibodies (Suppl. Figure 4a, b). These large plaque-associated dystrophic neurites (DN) were not labeled by anti-tau antibodies in control-injected or in non-injected 5xFAD mice (Fig. 2f, l). In contrast, many amyloid plaques showed DN positive for murine tau and oligomeric tau in their corona in the vicinity of the injection site in AD-PHF-injected 5xFAD mice (Fig. 2e, k). This was reflected by observing that the mean size of AD-PHF-induced tau-positive structures was significantly bigger in 5xFAD mice than in WT mice (Fig. 4a). The tau-positive area covered by these plaque-associated DN was significantly bigger than that of tau-positive inclusions at distance (more than 20 μm)

from amyloid deposits (Fig. 4b–d). The amyloid plaque burden in the cortex measured by image analysis was similar in 5xFAD mice injected with control material or with AD-PHF (Fig. 4e), and the levels of soluble and insoluble Aβ (Fig. 4f–h) were not significantly altered. Double immuno-labeling with B19 anti-tau and anti-APP antibodies showed occasional co-localization of tau and APP immunoreactivities in these globular processes around amyloid deposits (Suppl. Figure 4c–e). Triple staining for Aβ, tau and neurofilaments suggested their possible localization in the axonal prolongation in injected WT and 5xFAD mouse brains (Fig. 5a, d). Tau-positive processes were found in spherical or oval form or in the forms of NT around amyloid plaques (Suppl. video 1). 3D imaging confirmed that tau-positive processes adjacent to the plaques were much larger (Fig. 5b, e). Thus, human PHF induced accumulation of phosphorylated, conformationally abnormal and oligomeric mouse tau in dilated neuronal processes in the neuritic corona of amyloid plaques in 5xFAD mice and this was never seen in control-injected or in non-injected 5xFAD mice (Fig. 5c).

Insoluble tau and p25 levels are higher in AD-PHF-injected 5xFAD mice than in AD-PHF-injected WT mice

The level of soluble tau (Fig. 6a) was similar in 5xFAD mice injected with AD-PHF or with control fraction. The levels of AT8 and pS422 phosphotau were, however, significantly increased in the insoluble fraction of AD-PHF injected 5xFAD mice compared to control-injected 5xFAD mice (Fig. 6b, e, f). Despite the presence of tau inclusions in AD-PHF injected WT mice, the levels of insoluble phosphotau were not significantly increased in these mice. This may be related to a detection threshold unsensitive to a low abundance of local tau pathology in AD-PHF injected WT mouse cortex. Such a local tau pathology detected in a restricted cortical region may be less easily detectable when starting from homogenates of whole brain hemispheres for western blotting analysis. The p25 level and the p25/p35 ratio were significantly higher in AD-PHF-injected 5xFAD mice compared to AD-PHF-injected WT mice and to control-injected 5xFAD mice (Fig. 6c). The levels of CDK5 (Fig. 6d) and of several other protein kinases (GSK-3β, pGSK-3, ERK1/2, pERK, Fyn) (Suppl. Figure 5), and of proteosomal and autophagic markers (p62, β-catenin, LC3B) (Suppl. Figure 5), were not significantly altered.

The propagation of tau-positive aggregates is wider in AD-PHF-injected 5xFAD mice than in AD-PHF-injected WT mice

The anteroposterior propagation of tau inclusions in the ipsilateral cortex was estimated by the analysis of serial
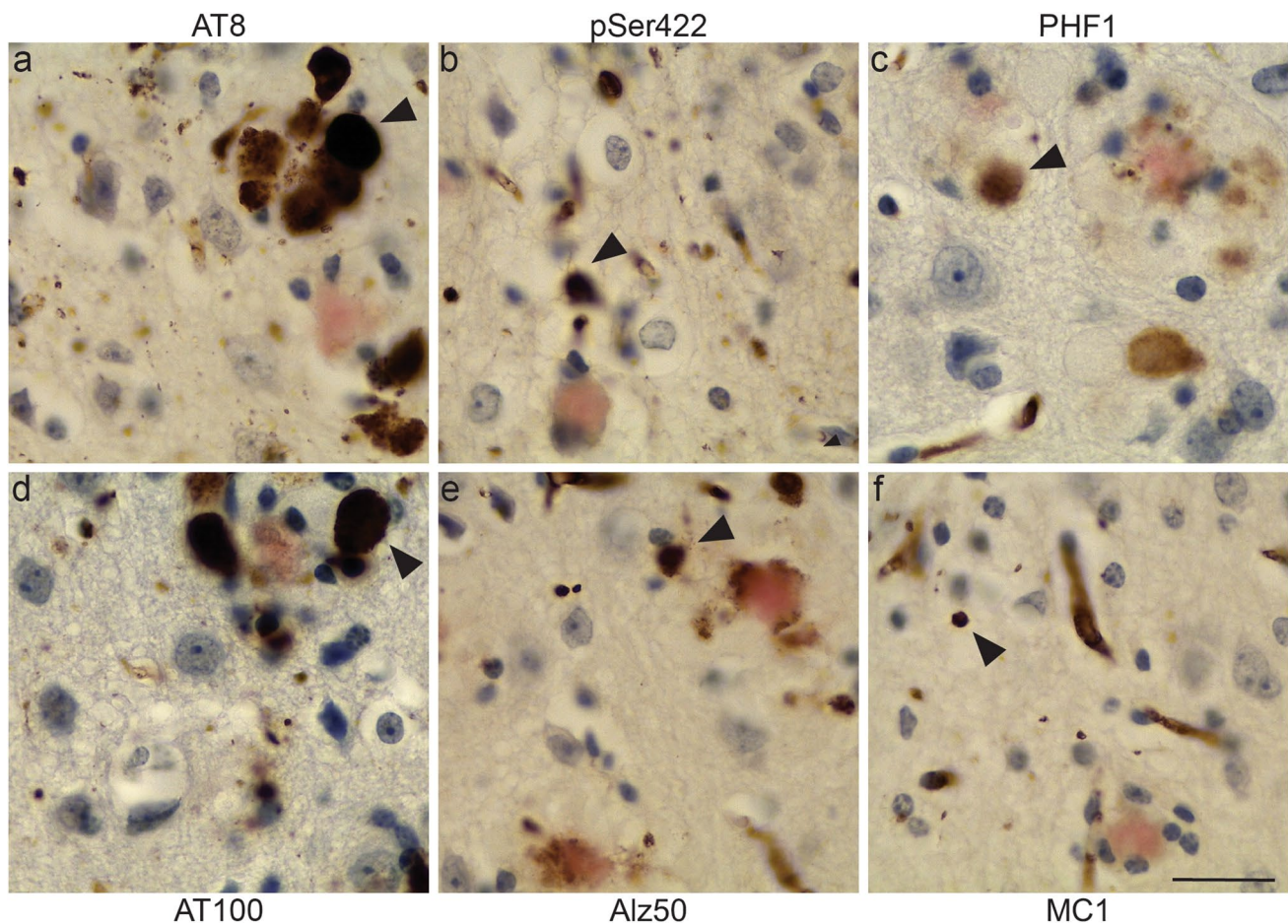
Fig. 3 Tau grains and plaque-associated dystrophic neurites in 5xFAD mice injected with AD-PHF are positive with antibodies to PHF-tau epitopes. Immunolabeling on tissue sections (cortex) of 5xFAD mice injected with AD-PHF. **a–c** Tau grains and plaque-associated dystrophic neurites (arrowheads) were positive with phos-photau antibodies AT8 (**a**), pSer422 (**b**) and PHF1 (**c**). **d–f** Tau grains and plaque-associated dystrophic neurites were positive with conformation dependent tau antibodies AT100 (**d**), Alz50 (**e**) and MC1 (**f**). Hematoxylin and Congo red counterstaining. Scale bar 20 μm

coronal sections (Fig. 7a–h). The maximal distance between anterior and posterior coronal levels where tau inclusions could be detected was significantly higher in 5xFAD mice (1770 μm ± 189 μm, mean ± SEM) than in WT mice (1158 μm ± 141.7 μm, mean ± SEM) (Fig. 7i). The anterior propagation from the injection site was higher in almost all the mice compared to posterior propagation behind the injection point (Fig. 7j, drawings in the first horizontal lane). Numerous tau grains and NT were also observed in the corpus callosum, both in WT and in 5xFAD mice (Fig. 7k, l). However, these tau inclusions barely ever crossed the midline in WT mice but crossed significantly more often the midline in 5xFAD mice (Fig. 7m). This contralateral propagation induced appearance of tau inclusions in the contralateral cortex in AD-PHF-injected 5xFAD mice, in mirror-image locations

(Fig. 7j, third horizontal lane) and not in AD-PHF-injected WT mice (Fig. 7j, second horizontal lane). Propagation of tau pathology outside of these cortical areas was not noticeable.

Tau-positive inclusions are composed of bundles of straight filaments

The ultrastructural features of tau pathology induced in 5xFAD mice by injection of human AD-PHF were also assessed on ultrathin sections with or without tau immunolabeling. In unlabeled ultrathin sections, granular inclusions were identified in the neuropil of AD-PHF-injected 5xFAD mice, and not in control-injected 5xFAD mice, as small ovoid processes limited by a plasma membrane and containing bundles of mostly straight, tightly packed filaments
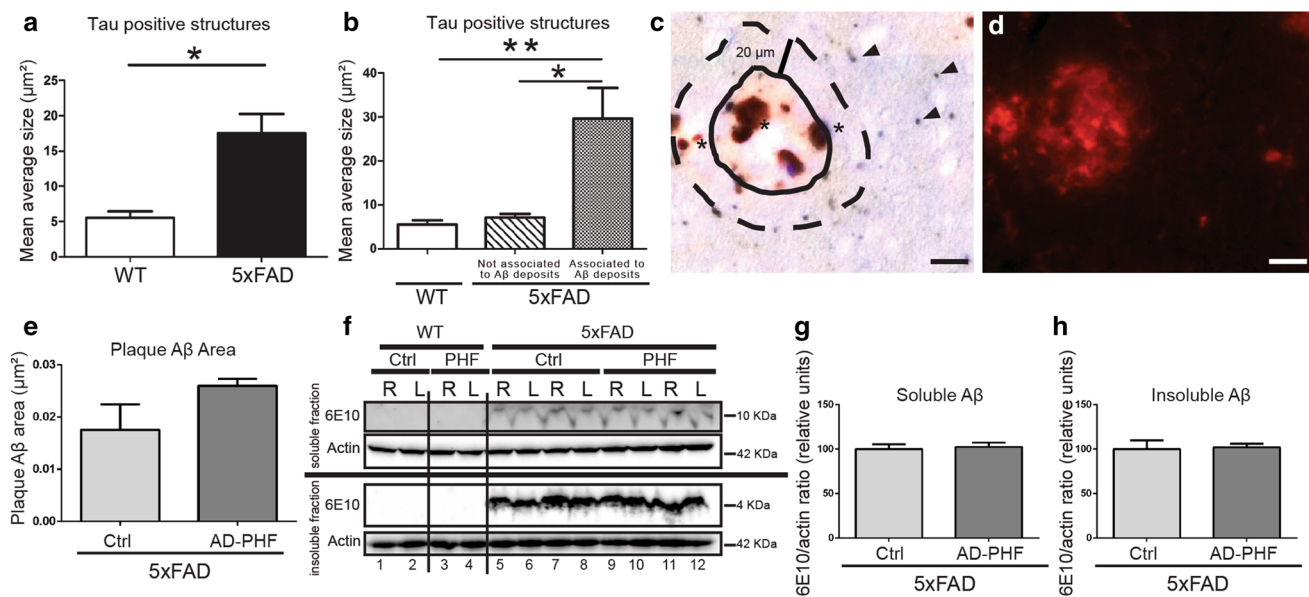
Fig. 4 Injection of AD-PHF induces the accumulation of tau into large plaque-associated dystrophic neurites in the cortex of 5xFAD mice. **a** The mean area covered by tau-positive structures (B19 anti-tau antibody) after injection of AD-PHF is significantly bigger in 5xFAD ($n=7$) mice than in WT ($n=6$) mice. **b** The mean area covered by tau-positive (B19 anti-tau antibody) structures associated with Aβ deposits (corresponding to plaque-associated DN) was significantly bigger than the mean area covered by tau-positive grains not associated with Aβ deposits in 5xFAD mice. **c, d** Double immunolabeling with tau (**c**, B19) and Aβ (**d**, 6E10) in a 5xFAD mouse injected with AD-PHF. The area covered by tau-positive processes in the neuritic plaque was measured in a total plaque surface (limited by the dashed line) extending 20 μm from the border of the Aβ deposit (limited by the solid line). The asterisks point on tau-positive plaque-associated DN. The arrowheads point on tau-positive grains not associated with Aβ deposits. **e** No significant difference was found after quantification of the area covered by Aβ deposits in the cortex of the injected mice at the level of the injection point. **f–h** The level of Aβ in the soluble (**g**) and the insoluble (**h**) fractions was not different in 5xFAD mice injected with control ($n=5$) (**f**, lanes 5–8) or AD-PHF ($n=7$) (**f**, lanes 9–12) (R right non-injected side, L left injected side). Actin was used as a control of charge. $*p < 0.05$; $**p < 0.01$. Unpaired two-tailed t test. Scale bar 25 μm

(Fig. 8a–c), with very occasional constrictions. These filaments had an apparent diameter of 20.5 nm ± 0.5 nm (mean ± SEM, $n=38$). Adjacent microtubules had an apparent diameter of 25.1 nm ± 0.6 nm (mean ± SEM, $n=23$) and adjacent neurofilaments an apparent diameter of 10.2 nm ± 1.1 nm (Fig. 8a). In tau-immunolabeled ultrathin sections, these filaments showed a strong tau immunoreactivity (Fig. 8d). The DN around amyloid deposits contained accumulations of autophagic vacuoles and lysosomal bodies both in non-injected and AD-PHF-injected 5xFAD mice (Suppl. Figure 6a, b). As in light microscopy, these dystrophic neurites showed tau immunoreactivity after immunolabeling of vibratome sections with the B19 anti-tau antibody (Suppl. Figure 6c). This tau immunoreactivity was diffuse or associated with autophagic vacuoles and lysosomal bodies and to very occasional filaments (Suppl. Figure 6d).

Discussion

In this study, we report that the brain propagation of tau pathology induced by injection of AD-PHF is accelerated in the presence of Aβ pathology, in the absence of non-physiological overexpression of FTDP-17 mutant tau, the latter paradigm having been used in most previous models [4, 5, 23, 27, 28, 36, 47, 48, 50, 51, 55]. Induction of tau aggregates in WT mice was previously observed after injection of AD brain homogenates [9, 49], and after injection of highly aggregated human wild-type tau in the form of PHF extracted from AD brain [3, 24]. We observed that AD-PHF initiates seeding of endogenous wild-type murine tau, not only in WT mice but also in 5xFAD and in APP$^{-/-}$ mice. Tau immunodepletion of AD-PHF fractions prevented the development and propagation of tau aggregates, indicating that human PHF was necessary to induce murine tau seeding. Also, injection of AD-PHF did not induce tau aggregates
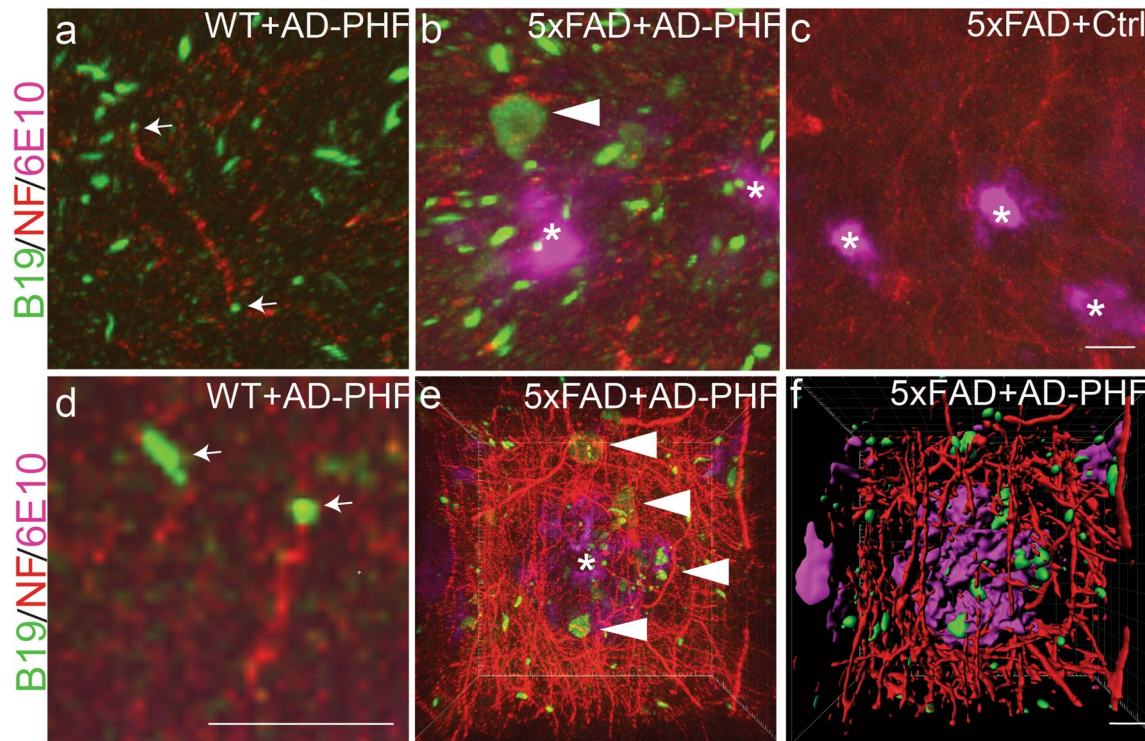
Fig. 5 Large and small tau-positive processes induced by injection of AD-PHF have distinct association with amyloid deposits and are associated with neuronal processes. 3D-imaging of triple immunolabeling with tau (B19, green), Aβ (6E10, purple) and NF (red) antibodies after CUBIC tissue clarification (WT-Ctrl: $n=1$, WT-AD-PHF: $n=1$, 5xFAD-Ctrl: $n=1$ and 5xFAD-AD-PHF: $n=2$). **a**, **d** Small tau-positive grains or threads (small arrows) were detected in continuity with NF positive axonal processes in WT mice injected with AD-PHF. Single-plane image. **b**, **c** Large tau-positive DN (big arrowheads) develop around amyloid core (white asterisks) in plaques in 5xFAD mice injected with AD-PHF (**b**) but not after injection of control fraction (**c**). Single-plane image. **e**, **f** 3D-rendering of triple labeling in 5xFAD mice injected with AD-PHF (Z stack: 1 μm step×79 planes). Large tau-positive DN (big arrowheads) are closely adjacent to amyloid deposit (asterisk). Surface smoothed image of **e** is shown in **f**. Scale bars 10 μm

in tau$^{-/-}$ mice indicating that murine tau was necessary to initiate the formation and the propagation of these aggregates. We show for the first time by ultrastructural analysis that endogenous wild-type tau aggregates induced by in vivo seeding with exogenous human PHF are made of filaments. Tau filaments in human tauopathies show various morphologies [13]. Human AD filaments, made of 3R and 4R tau isoforms, consist mostly of PHF with a width alternating between 8 to 20 nm with a longitudinal cross-over spacing of 80 nm [12, 32, 54] and more rarely of straight 15 nm wide straight filaments [12]; both are considered to be ultrastructural polymorphs [20]. In several human tauopathies characterized by the presence of tau aggregates made of 4R tau isoforms, such as in progressive supranuclear palsy, neurofibrillary tangles are also composed of 15 nm straight filaments [16]. In vitro, human AD-tau filaments seed aggregation of 4R recombinant tau into filaments made only of 4R tau [24] and 4R tau isoforms assemble into straight filaments [22]. Since only 4R tau isoforms are expressed in the adult murine brain [30], seeding by human AD-PHF would conceivably lead to their assembly mostly in straight filaments.

Interestingly, human PHF extracted from AD cases and showing seeding ability had an average length (180 nm) quite similar to the average length of tau fibrils (179 nm) with the highest seeding competency extracted from the brain of P301S tau mice [29], confirming that large tau assemblies in the form of short tau fibrils are potent at seeding tau aggregation, including heterotopic seeding of mouse tau. These AD-PHF showed partial resistance to proteinase K digestion generating smaller tau fragments with molecular weights between 15 and 20 kDa as reported in other studies [41, 53], confirming that the seeding ability of AD-PHF is associated with a conformation of these tau assemblies conferring this protease resistance [31].

Our observation of increased propagation of tau pathology in the presence of Aβ pathology is made in a model not overexpressing mutant tau protein and where non-mutant tau is expressed at a physiological level and is exposed to Aβ, mimicking more faithfully sporadic
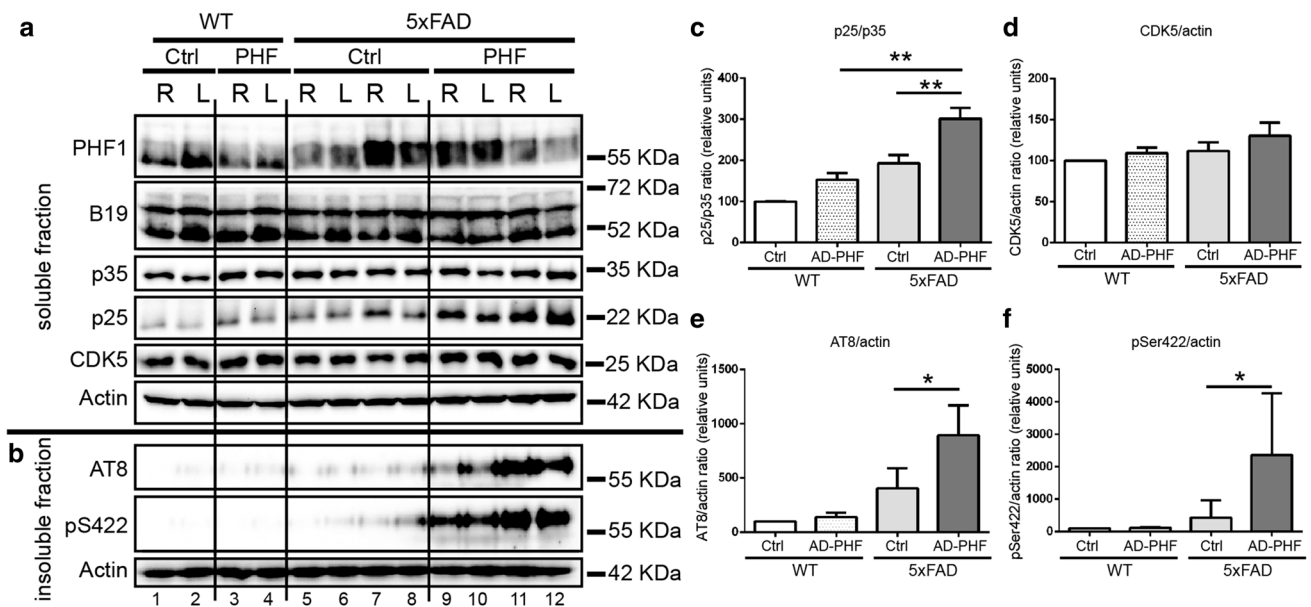
Fig. 6 Levels of insoluble phosphotau and of p25 are higher in 5xFAD mice than in WT mice after injection of AD-PHF. Representative western blots of the soluble (**a**) and the insoluble (**b**) brain fractions (*R* right non-injected side, *L* left injected side) from WT (lanes 1–4) and 5xFAD (lanes 5–12) mice, injected with control fraction (Ctrl) and AD-PHF (WT-Ctrl: $n=3$; WT-AD-PHF: $n=4$; 5xFAD-Ctrl: $n=5$; 5xFAD-AD-PHF: $n=7$). **a** The level of total tau (B19) and of phosphotau (PHF1) in the RIPA soluble fraction was not different between WT and 5xFAD mice injected with control fraction or AD-PHF. The level of p25 was increased in AD-PHF-injected 5xFAD mice (lanes 9–12). **b** The level of phosphotau (AT8, pS422) was markedly increased in the RIPA insoluble fraction of AD-PHF-injected 5xFAD mice (lanes 9–12) compared to AD-PHF-injected WT mice (lanes 3 and 4) or control-injected 5xFAD mice (lanes 5–8). Actin was used as a control of charge. **c** The p25/p35 ratio was increased in 5xFAD mice injected with AD-PHF, compared to injection with control fraction and was also significantly higher in AD-PHF-injected 5xFAD compared to AD-PHF-injected WT. **d** The levels of CDK5 were not significantly different between WT and 5xFAD mice. **e, f** Insoluble phosphotau levels analyzed using AT8 and pSer422 antibodies were significantly higher in AD-PHF injected 5xFAD mice than in control injected 5xFAD mice. *$p < 0.05$; **$p < 0.01$. Two-way ANOVA

late-onset AD. We observed both an ipsilateral and a contralateral enhancement of tau propagation in the cortex in AD-PHF-injected 5xFAD mice compared to AD-PHF-injected WT mice. Ipsilateral anteroposterior propagation of murine tau aggregates in the cortex suggests the involvement of long-distance associative intrahemispheric projection neurons [15]. Contralateral propagation across the midline suggests involvement of commissural projection neurons, mostly callosal projection neurons sending axons through the corpus callosum to mirror-image locations of the contralateral hemisphere. In addition, local connections by cortical interneurons might be involved.

This enhanced tau propagation in 5xFAD mice might reflect the reported ability of aggregation-prone proteins to induce heterotopic cross-seeding. E.g., α-synuclein pre-formed filaments increased tau aggregation in vitro, in primary neurons and in mutant transgenic mice [21]. A direct binding between Aβ peptides and tau that might accelerate self-aggregation of both has been reported in vitro [25] and in silico models [38]. Aβ42

or α-synuclein oligomers can indeed seed recombinant tau to generate tau oligomers [33]. In vitro fibrillization of recombinant mutant tau by pre-aggregated Aβ and increased tau spreading after injection of this Aβ-seeded tau in mutant tau mice has been demonstrated [58], suggesting that Aβ can accelerate the generation of tau fibrils with seeding property. Aβ accumulates intracellularly in neurons in 5xFAD mice in an aggregated state [44] where it could directly interact with human tau seeds and favor heterotopic seeding of mouse tau. Increased levels of p25 and of the p25/p35 ratio, p25 being converted from p35 via proteolysis by calpain and being a constitutive activator of CDK5, were observed in AD-PHF-injected 5xFAD mice and this might also be a mechanism driving enhanced tau pathology. CDK5 activation by p25 was reported to favor tau phosphorylation and aggregation [14, 43] and p25 accumulates in AD brain [46] and in APP mice [45]. Further studies will, however, be necessary to establish the relationship between these changes
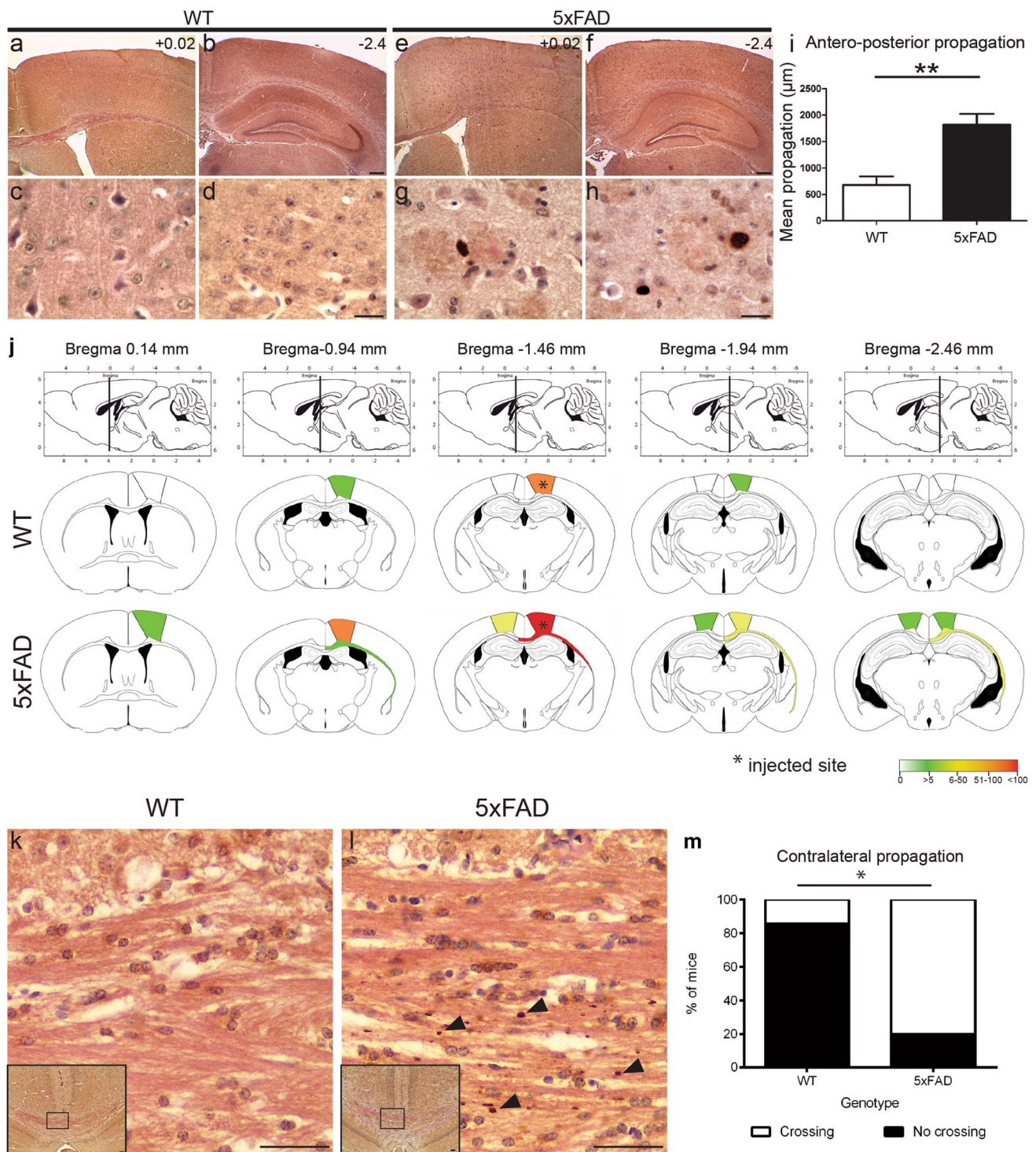
in p25 levels and tau aggregation in AD-PHF-injected 5xFAD mice.

A remarkable effect of injection of human AD-PHF in 5xFAD mice was the appearance of enlarged phospho-tau positive, plaque-associated dystrophic neurites (DN)

◄**Fig. 7** Increased propagation of induced tau aggregates in 5xFAD mice compared to WT mice. Immunohistochemical labeling with the B19 anti-tau antibody on coronal sections at similar anterior (**a**, **e**) and posterior (**b**, **f**) levels (according to Bregma level from Paxinos atlas) after injection of AD-PHF in WT and 5xFAD mice. **a–d** B19 tau immunolabeling in AD-PHF-injected WT mouse brain. Tau pathology was absent in the cortex of this WT mouse at these anterior (**a**) and posterior (**b**) levels (shown at higher magnification in **c** and **d**). **e–h** B19 tau immunolabeling in AD-PHF-injected 5xFAD mouse brain. A tau pathology was present at anterior (**e**) and posterior (**f**) levels in this 5xFAD mouse (shown at higher magnification in **g** and **h**, as plaque-associated tau-positive DN). Scale bars: 250 μm for **a**, **b**, **e**, **f** and 20 μm for **c**, **d**, **g**, **h**. **i** The mean anteroposterior propagation of tau pathology was significantly higher in 5xFAD mice compared to WT mice. **p < 0.01, unpaired two-tailed *t* test. **j** Propagation of tau pathology at five different anatomical levels, corresponding to five different bregma levels (0.14, −0.94, −1.46, −1.94 and −2.46 mm) (drawings in the first horizontal lane). Heat maps representation of the distribution and density of tau pathology in representative WT (second horizontal lane) and 5xFAD (third horizontal lane) mice injected with AD-PHF in the somatosensory cortex (asterisks). Tau pathology was graded using B19 total tau antibody at these 5 different anatomical levels. Tau pathology propagation in 5xFAD mice was greater, being present in the corpus callosum and expanding into the contralateral non-injected site. **k**, **l** Tau-positive grains were present in axons in the corpus callosum after injection of AD-PHF into the overlying cortex and were crossing the midline in a 5xFAD mouse (**l**) but not in a WT mouse (**k**). Insets show the localization of panels k and l at lower magnification. Hematoxylin counterstaining. Scale bars 50 μm. **m** Chi square analysis of the percentage of AD-PHF-injected WT and 5xFAD mice showing (white) or not (black) a tau pathology crossing the midline in the corpus callosum. AD-PHF-injected 5xFAD mice showed a significant increased contralateral propagation (**p = 0.015 by Fisher's exact test)

in many neuritic plaques near and at distance from the injection site. In non-injected or control-injected 5xFAD mouse brains, large plaque-associated DN were present but were rarely detected with tau antibodies at 9 months. The tau immunoreactivity induced by AD-PHF in these DN was diffusely distributed between autophagosomes/lysosomal bodies or associated with their content; these DN were not labeled by human tau-specific antibodies, indicating that the appearance of tau-positive plaque-associated DN did not result from internalized human PHF. These plaque-associated DN were positive with the anti-oligomeric tau T22 antibody suggesting that AD-PHF induced the formation of murine tau oligomers in DN.

While finalizing this article, enhancement of tau pathology in amyloid models by injection of AD-tau was reported [26]. Our present data are in general agreement with these data, providing some more detailed morphological information on the ultrastructure of AD-PHF-induced tau pathology. In the latter study, hippocampal injection of AD-PHF in 5xFAD mice induced the development of tau aggregates in DN surrounding amyloid deposits, NFTs and NT, but with a temporal sequence: aggregated tau in DN surrounding amyloid deposits was seen as the first lesion with no or minimal NFTs and NT at 3 months post-injection. In the present study, tau-positive plaque-associated DN, grains and NT were observed together at 3 months post-injection. In addition, abundant large tau-positive plaque-associated DN (not punctuate small tau-positive neurites) were not seen in non-injected 5xFAD mice in our study. Some differences between both studies might be related to the distinct experimental designs, such as PHF preparation protocols, age at injection, post-incubation length, and the injection site (hippocampus versus cortex). The increased tau pathology observed in injected 5xFAD mice cannot unequivocally be attributed only to the production of Aβ, since these mice also overexpress FAD mutant APP and PS1 proteins. APP or its physiological proteolytic products might play a role in the observed increased tau pathology. Overexpression of mutant APP [37] or PS1 [6] increases tau phosphorylation that might favor murine tau seeding in presence of injected human tau seeds. APP (or its fragments) by itself is, however, not necessary for murine tau seeding by human tau seeds since we still observed pathological tau spreading in APP$^{-/-}$ mice.

This enhancement of tau propagation induced by Aβ might be an essential mechanism driving expansion of tau lesions during the progression of AD. Tau lesions, with or without minimal Aβ deposition, are initially limited to entorhinal cortex and hippocampus either as a "Primary Age-related tauopathy" (PART) [11] or as an early AD stage [17], but severe enhancement and spreading of tau lesions occurs at later stages when most often tau and Aβ lesions co-exist. Our experimental data support the idea that spreading of pre-existing tau pathology in limited brain areas in AD is enhanced by Aβ pathology
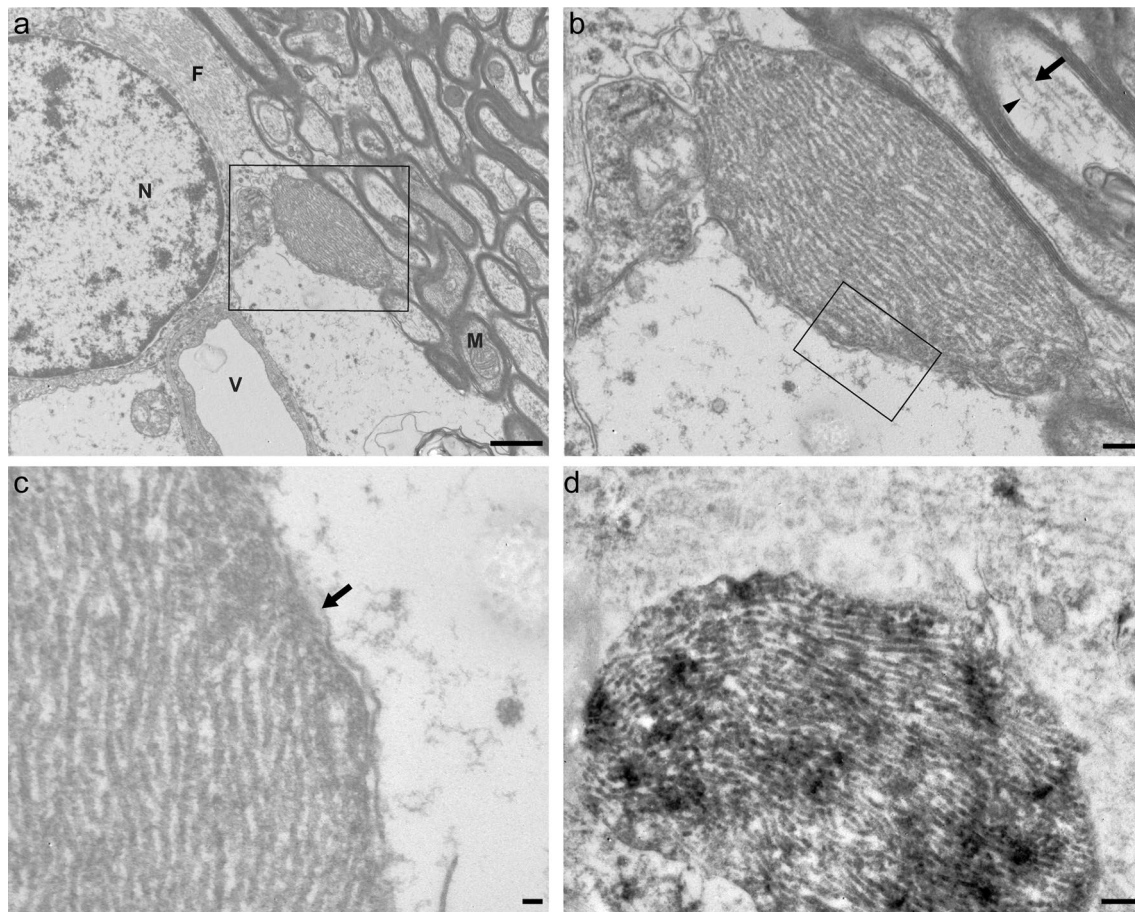
Fig. 8 Ultrastructural aspect of murine tau filaments seeded in vivo by AD-PHF. Ultrathin sections (cerebral cortex, near the corpus callosum) showing the structure of tau aggregates in 5xFAD mice injected with AD-PHF. **a** Granular inclusions (as shown inside the rectangular area) were identified in the neuropil of AD-PHF-injected 5xFAD mice, and not in control-injected 5xFAD mice. The granular inclusion is adjacent to myelinated axons containing mitochondria (M) and near an astrocyte showing its nucleus (N) and glial intermediary filaments in its cytoplasm (F). A blood capillary (V) is also visible. **b** Higher magnification of the rectangular area in **a** showing that this inclusion contains bundles of closely adjacent filaments. The arrow points to an adjacent microtubule and the arrowhead to a neurofilament for comparison. **c** Higher magnification of the rectangular area in **b** shows that these filaments are mostly straight and 20 nm wide. The inclusion was surrounded by a membrane (arrow). **d** Ultrathin section of a vibratome section immunolabeled with the B19 tau antibody (DAB method). The filaments in this inclusion were tau positive (black deposit of DAB polymerization product). Scale bars **a** 1 μm; **b**, **d** 0.2 μm; **c** 0.05 μm

through enhanced prion-like mechanisms of pathological tau seeding.

References

1. Ando K, Laborde Q, Brion JP, Duyckaerts C (2018) 3D imaging in the postmortem human brain with CLARITY and CUBIC. Handb Clin Neurol 150:303–317. https://doi.org/10.1016/B978-0-444-63639-3.00021-9
2. Ando K, Tomimura K, Sazdovitch V, Suain V, Yilmaz Z, Authelet M et al (2016) Level of PICALM, a key component of clathrin-mediated endocytosis, is correlated with levels of phosphotau and autophagy-related proteins and is associated with tau inclusions in AD, PSP and Pick disease. Neurobiol Dis 94:32–43. https://doi.org/10.1016/j.nbd.2016.05.017
3. Audouard E, Houben S, Masaracchia C, Yilmaz Z, Suain V, Authelet M et al (2016) High-molecular-weight paired helical filaments from Alzheimer brain induces seeding of wild-type mouse

tau into an argyrophilic 4R tau pathology in vivo. Am J Pathol 186:2709–2722. https://doi.org/10.1016/j.ajpath.2016.06.008

4. Bennett RE, DeVos SL, Dujardin S, Corjuc B, Gor R, Gonzalez J et al (2017) Enhanced tau aggregation in the presence of amyloid β. Am J Pathol 187:1601–1612. https://doi.org/10.1016/j.ajpath.2017.03.011

5. Bolmont T, Clavaguera F, Meyer-Luehmann M, Herzig MC, Radde R, Staufenbiel M et al (2007) Induction of tau pathology by intracerebral infusion of amyloid-beta -containing brain extract and by amyloid-beta deposition in APP × Tau transgenic mice. Am J Pathol 171:2012–2020. https://doi.org/10.2353/ajpath.2007.070403

6. Boutajangout A, Leroy K, Touchet N, Authelet M, Blanchard V, Tremp G et al (2002) Increased tau phosphorylation but absence of formation of neurofibrillary tangles in mice double transgenic for human tau and Alzheimer mutant (M146L) presenilin-1. Neurosci Lett 318:29–33

7. Braak H, Braak E (1991) Neuropathological stageing of Alzheimer-related changes. Acta Neuropathol 82:239–259

8. Brion JP, Hanger DP, Couck AM, Anderton BH (1991) A68 proteins in Alzheimer's disease are composed of several tau isoforms in a phosphorylated state which affects their electrophoretic mobilities. Biochem J 279(Pt 3):831–836

9. Clavaguera F, Akatsu H, Fraser G, Crowther RA, Frank S, Hench J et al (2013) Brain homogenates from human tauopathies induce tau inclusions in mouse brain. Proc Natl Acad Sci USA 110:9535–9540. https://doi.org/10.1073/pnas.1301175110

10. Clavaguera F, Hench J, Goedert M, Tolnay M (2015) Invited review: prion-like transmission and spreading of tau pathology. Neuropathol Appl Neurobiol 41:47–58. https://doi.org/10.1111/nan.12197

11. Crary JF, Trojanowski JQ, Schneider JA, Abisambra JF, Abner EL, Alafuzoff I et al (2014) Primary age-related tauopathy (PART): a common pathology associated with human aging. Acta Neuropathol 128:755–766. https://doi.org/10.1007/s00401-014-1349-0

12. Crowther RA (1991) Straight and paired helical filaments in Alzheimer disease have a common structural unit. Proc Natl Acad Sci USA 88:2288–2292

13. Crowther RA, Goedert M (2000) Abnormal tau-containing filaments in neurodegenerative diseases. J Struct Biol 130:271–279. https://doi.org/10.1006/jsbi.2000.4270

14. Cruz JC, Tseng HC, Goldman JA, Shih H, Tsai LH (2003) Aberrant Cdk5 activation by p25 triggers pathological events leading to neurodegeneration and neurofibrillary tangles. Neuron 40:471–483

15. Custo Greig LF, Woodworth MB, Galazo MJ, Padmanabhan H, Macklis JD (2013) Molecular logic of neocortical projection neuron specification, development and diversity. Nat Rev Neurosci 14:755–769. https://doi.org/10.1038/nrn3586

16. Dickson DW, Rademakers R, Hutton ML (2007) Progressive supranuclear palsy: pathology and genetics. Brain Pathol 17:74–82. https://doi.org/10.1111/j.1750-3639.2007.00054.x

17. Duyckaerts C, Braak H, Brion JP, Buee L, Del Tredici K, Goedert M et al (2015) PART is part of Alzheimer disease. Acta Neuropathol 129:749–756. https://doi.org/10.1007/s00401-015-1390-7

18. Duyckaerts C, Delatour B, Potier MC (2009) Classification and basic pathology of Alzheimer disease. Acta Neuropathol 118:5–36. https://doi.org/10.1007/s00401-009-0532-1

19. Falcon B, Cavallini A, Angers R, Glover S, Murray TK, Barnham L et al (2015) Conformation determines the seeding potencies of native and recombinant Tau aggregates. J Biol Chem 290:1049–1065. https://doi.org/10.1074/jbc.M114.589309

20. Fitzpatrick AWP, Falcon B, He S, Murzin AG, Murshudov G, Garringer HJ et al (2017) Cryo-EM structures of tau filaments from Alzheimer's disease. Nature 547:185–190. https://doi.org/10.1038/nature23002

21. Giasson BI, Forman MS, Higuchi M, Golbe LI, Graves CL, Kotzbauer PT et al (2003) Initiation and synergistic fibrillization of tau and alpha-synuclein. Science 300:636–640. https://doi.org/10.1126/science.1082324

22. Goedert M, Jakes R, Spillantini MG, Hasegawa M, Smith MJ, Crowther RA (1996) Assembly of microtubule-associated protein tau into Alzheimer-like filaments induced by sulphated glycosaminoglycans. Nature 383:550–553. https://doi.org/10.1038/383550a0

23. Gotz J, Chen F, van Dorpe J, Nitsch RM (2001) Formation of neurofibrillary tangles in P301 l tau transgenic mice induced by Abeta 42 fibrils. Science 293:1491–1495. https://doi.org/10.1126/science.1062097

24. Guo JL, Narasimhan S, Changolkar L, He Z, Stieber A, Zhang B et al (2016) Unique pathological tau conformers from Alzheimer's brains transmit tau pathology in nontransgenic mice. J Exp Med 213:2635–2654. https://doi.org/10.1084/jem.20160833

25. Guo JP, Arai T, Miklossy J, McGeer PL (2006) Abeta and tau form soluble complexes that may promote self aggregation of both into the insoluble forms observed in Alzheimer's disease. Proc Natl Acad Sci USA 103:1953–1958. https://doi.org/10.1073/pnas.0509386103

26. He Z, Guo JL, McBride JD, Narasimhan S, Kim H, Changolkar L et al (2018) Amyloid-beta plaques enhance Alzheimer's brain tau-seeded pathologies by facilitating neuritic plaque tau aggregation. Nat Med 24:29–38. https://doi.org/10.1038/nm.4443

27. Héraud C, Goufak D, Ando K, Leroy K, Suain V, Yilmaz Z et al (2014) Increased misfolding and truncation of tau in APP/PS1/tau transgenic mice compared to mutant tau mice. Neurobiol Dis 62:100–112. https://doi.org/10.1016/j.nbd.2013.09.010

28. Hurtado DE, Molina-Porcel L, Iba M, Aboagye AK, Paul SM, Trojanowski JQ et al (2010) A{beta} accelerates the spatiotemporal progression of tau pathology and augments tau amyloidosis in an Alzheimer mouse model. Am J Pathol 177:1977–1988. https://doi.org/10.2353/ajpath.2010.100346

29. Jackson SJ, Kerridge C, Cooper J, Cavallini A, Falcon B, Cella CV et al (2016) Short fibrils constitute the major species of seed-competent tau in the brains of mice transgenic for human P301S tau. J Neurosci 36:762–772. https://doi.org/10.1523/JNEUROSCI.3542-15.2016

30. Janke C, Beck M, Stahl T, Holzer M, Brauer K, Bigl V et al (1999) Phylogenetic diversity of the expression of the microtubule-associated protein tau: implications for neurodegenerative disorders. Brain Res Mol Brain Res 68:119–128

31. Kaufman SK, Sanders DW, Thomas TL, Ruchinskas AJ, Vaquer-Alicea J, Sharma AM et al (2016) Tau prion strains dictate patterns of cell pathology, progression rate, and regional vulnerability in vivo. Neuron 92:796–812. https://doi.org/10.1016/j.neuron.2016.09.055

32. Kidd M (1963) Paired helical filaments in electron microscopy of Alzheimer's disease. Nature 197:192–193. https://doi.org/10.1038/197192b0

33. Lasagna-Reeves CA, Castillo-Carranza DL, Guerrero-Muoz MJ, Jackson GR, Kayed R (2010) Preparation and characterization of neurotoxic tau oligomers. Biochemistry 49:10039–10041. https://doi.org/10.1021/bi1016233

34. Leroy K, Ando K, Heraud C, Yilmaz Z, Authelet M, Boeynaems JM et al (2010) Lithium treatment arrests the development of neurofibrillary tangles in mutant tau transgenic mice with advanced neurofibrillary pathology. J Alzheimers Dis 19:705–719. https://doi.org/10.3233/JAD-2010-1276

35. Leroy K, Ando K, Laporte V, Dedecker R, Suain V, Authelet M et al (2012) Lack of tau proteins rescues neuronal cell death and decreases amyloidogenic processing of APP in APP/PS1 mice. Am J Pathol 181:1928–1940. https://doi.org/10.1016/j.ajpath.2012.08.012

36. Lewis J, Dickson DW, Lin WL, Chisholm L, Corral A, Jones G et al (2001) Enhanced neurofibrillary degeneration in transgenic mice expressing mutant tau and APP. Science 293:1487–1491. https://doi.org/10.1126/science.1058189

37. Masliah E, Sisk A, Mallory M, Games D (2001) Neurofibrillary pathology in transgenic mice overexpressing V717F beta-amyloid precursor protein. J Neuropathol Exp Neurol 60:357–368

38. Miller Y, Ma B, Nussinov R (2011) Synergistic interactions between repeats in tau protein and Abeta amyloids may be responsible for accelerated aggregation via polymorphic states. Biochemistry 50:5172–5181. https://doi.org/10.1021/bi200400u

39. Morel M, Authelet M, Dedecker R, Brion JP (2010) Glycogen synthase kinase-3beta and the p25 activator of cyclin dependent kinase 5 increase pausing of mitochondria in neurons. Neuroscience 167:1044–1056. https://doi.org/10.1016/j.neuroscience.2010.02.077

40. Mudher A, Colin M, Dujardin S, Medina M, Dewachter I, Naini SMA et al (2017) What is the evidence that tau pathology spreads through prion-like propagation? Acta Neuropathol Commun 5:99. https://doi.org/10.1186/s40478-017-0488-7

41. Narasimhan S, Guo JL, Changolkar L, Stieber A, McBride JD, Silva LV et al (2017) Pathological tau strains from human brains recapitulate the diversity of tauopathies in nontransgenic mouse brain. J Neurosci 37:11406–11423. https://doi.org/10.1523/JNEUROSCI.1230-17.2017

42. Nelson PT, Alafuzoff I, Bigio EH, Bouras C, Braak H, Cairns NJ et al (2012) Correlation of Alzheimer disease neuropathologic changes with cognitive status: a review of the literature. J Neuropathol Exp Neurol 71:362–381. https://doi.org/10.1097/NEN.0b013e31825018f7

43. Noble W, Olm V, Takata K, Casey E, Mary O, Meyerson J et al (2003) Cdk5 is a key factor in tau aggregation and tangle formation in vivo. Neuron 38:555–565

44. Oakley H, Cole SL, Logan S, Maus E, Shao P, Craft J et al (2006) Intraneuronal beta-amyloid aggregates, neurodegeneration, and neuron loss in transgenic mice with five familial Alzheimer's disease mutations: potential factors in amyloid plaque formation. J Neurosci 26:10129–10140

45. Otth C, Concha II, Arendt T, Stieler J, Schliebs R, Gonzalez-Billault C et al (2002) AbetaPP induces cdk5-dependent tau hyperphosphorylation in transgenic mice Tg2576. J Alzheimers Dis 4:417–430

46. Patrick GN, Zukerberg L, Nikolic M, de la Monte S, Dikkes P, Tsai LH (1999) Conversion of p35 to p25 deregulates Cdk5 activity and promotes neurodegeneration. Nature 402:615–622. https://doi.org/10.1038/45159

47. Perez M, Ribe E, Rubio A, Lim F, Moran MA, Ramos PG et al (2005) Characterization of a double (amyloid precursor protein-tau) transgenic: tau phosphorylation and aggregation. Neuroscience 130:339–347. https://doi.org/10.1016/j.neuroscience.2004.09.029

48. Pooler AM, Polydoro M, Maury EA, Nicholls SB, Reddy SM, Wegmann S et al (2015) Amyloid accelerates tau propagation and toxicity in a model of early Alzheimer's disease. Acta Neuropathol Commun 3:14. https://doi.org/10.1186/s40478-015-0199-x

49. Sanders DW, Kaufman SK, Holmes BB, Diamond MI (2016) Prions and protein assemblies that convey biological information in health and disease. Neuron 89:433–448. https://doi.org/10.1016/j.neuron.2016.01.026

50. Seino Y, Kawarabayashi T, Wakasaya Y, Watanabe M, Takamura A, Yamamoto-Watanabe Y et al (2010) Amyloid beta accelerates phosphorylation of tau and neurofibrillary tangle formation in an amyloid precursor protein and tau double-transgenic mouse model. J Neurosci Res 88:3547–3554. https://doi.org/10.1002/jnr.22516

51. Stancu IC, Ris L, Vasconcelos B, Marinangeli C, Goeminne L, Laporte V et al (2014) Tauopathy contributes to synaptic and cognitive deficits in a murine model for Alzheimer's disease. FASEB J 28:2620–2631. https://doi.org/10.1096/fj.13-246702

52. Susaki EA, Tainaka K, Perrin D, Kishino F, Tawara T, Watanabe TM et al (2014) Whole-brain imaging with single-cell resolution using chemical cocktails and computational analysis. Cell 157:726–739. https://doi.org/10.1016/j.cell.2014.03.042

53. Taniguchi-Watanabe S, Arai T, Kametani F, Nonaka T, Masuda-Suzukake M, Tarutani A et al (2016) Biochemical classification of tauopathies by immunoblot, protein sequence and mass spectrometric analyses of sarkosyl-insoluble and trypsin-resistant tau. Acta Neuropathol 131:267–280. https://doi.org/10.1007/s00401-015-1503-3

54. Terry RD (1963) The fine structure of neurofibrillary tangles in Alzheimer's disease. J Neuropathol Exp Neurol 22:629–642

55. Terwel D, Muyllaert D, Dewachter I, Borghgraef P, Croes S, Devijver H et al (2008) Amyloid activates GSK-3beta to aggravate neuronal tauopathy in bigenic mice. Am J Pathol 172:786–798. https://doi.org/10.2353/ajpath.2008.070904

56. Tucker KL, Meyer M, Barde YA (2001) Neurotrophins are required for nerve growth during development. Nat Neurosci 4:29–37

57. Vanden Dries V, Stygelbout V, Pierrot N, Yilmaz Z, Suain V, De Decker R et al (2017) Amyloid precursor protein reduction enhances the formation of neurofibrillary tangles in a mutant tau transgenic mouse model. Neurobiol Aging 55:202–212. https://doi.org/10.1016/j.neurobiolaging.2017.03.031

58. Vasconcelos B, Stancu IC, Buist A, Bird M, Wang P, Vanoosthuyse A et al (2016) Heterotypic seeding of Tau fibrillization by pre-aggregated Abeta provides potent seeds for prion-like seeding and propagation of Tau-pathology in vivo. Acta Neuropathol 131:549–569. https://doi.org/10.1007/s00401-015-1525-x

59. Zheng H, Jiang M, Trumbauer ME, Sirinathsinghji DJ, Hopkins R, Smith DW et al (1995) beta-Amyloid precursor protein-deficient mice show reactive gliosis and decreased locomotor activity. Cell 81:525–531